

Type-II GaInAsSb/InP Modified Uni-Traveling Carrier Photodiodes Under Zero-Bias Operation

Rimjhim Chaudhary,¹ Akshay M. Arabhavi,¹ Sara Hamzeloui,¹ Martin Leich,¹ Olivier Ostinelli,¹ and Colombo R. Bolognesi,^{1,*}

¹ ETH Zurich, Millimeter-Wave Electronics Laboratory (MWE), 8092 Zürich, Switzerland

*bcolombo@mwe.ee.ethz.ch

Abstract: We report the first bias-free performance of Type-II modified GaInAsSb/InP UTC-PD for high-bandwidth and high-power applications. The UTC-PD achieves zero-bias bandwidth of 60 GHz and high output power of -11 dBm at 100 GHz. © 2023 The Author(s)

1. Introduction

Millimeter-wave signal generation has seen a significant shift toward photonic-based technologies, thanks to their wide bandwidth, high output power, and compact form factor. These features have made them invaluable in diverse fields, including radar technology, sub-THz wireless communications, *etc* [1]. An essential element of such systems is the optical-to-electrical (O/E) signal interface, such as high-bandwidth and high-power photodiodes. High-power application of the PD is desirable as it eliminates the need for high-bandwidth post-amplification electronics thus extending the bandwidth of the entire system [2]. Moreover, the bias-free operation of UTC-PDs is also crucial to reducing the requirement for numerous bias feeds, simplifying biasing effects, and minimizing electrical cross-talks. Eliminating the power supply leads to a simpler design, reduced heat generation, improved reliability, lower power consumption, and decreased overall operational costs [3,4].

Uni-traveling carrier photodiodes (UTC-PD) involving only the transport of fast-moving carriers (electrons) are a good candidate for high-bandwidth and high-power operations. This effectively eliminates the long tail response and space charge effect inherent in hole drift transport within PIN-PDs [2,5]. With their heavily *p*-doped absorber and lightly *n*-doped collector layer, UTC-PDs have a sufficient electric field for efficient electron transport making them an ideal candidate for bias-free operation [3,4]. High 3-dB bandwidths of 310 GHz [5] and output power reaching 20 mW at 100 GHz [2] have been successfully achieved in UTC-PDs incorporating a graded GaInAs absorber layer and use of resonating matching circuits. Additionally, a zero-bias bandwidth of 170 GHz and an output power of -11.3 dBm at 170 GHz have been demonstrated in a Type-II (GaAs_{0.5}Sb_{0.5}/InP) UTC-PD, with a modified graded collector layer consisting of InP and In_{0.52}Al_xGa_{0.48-x}As [6].

The conduction band discontinuity of $\Delta E_C = 0.25$ eV between a GaInAs absorber and an InP collector, impedes electron transport from the absorber to the collector. Regardless of various schemes *e.g.*, step-grading [2] or chirped-superlattice [7], the traveling space charge of electrons at high excitation eventually leads to the collapse of the electric field in the collector and limits the high-power capability of the devices. GaInAs-based UTC-PDs exhibit low saturation currents at zero-bias, leading to reduced overall RF output power [3,8]. Type-II UTC-PDs with a GaAsSb absorber are good candidates for high-power operations, but their transit-limited bandwidth is restricted due to the low electron mobility in GaAsSb [9]. Moreover, GaAsSb has a relatively low Γ -L conduction band intervalley separation, leading to a significant number of electrons residing in the less mobile satellite valleys, even at moderate levels of electron injection. The GaAsSb L-valley sits at a lower conduction band level compared to InP, creating a Type-I band discontinuity that acts as a barrier, impeding the flow of electrons from GaAsSb to InP. Adding In- to the GaAsSb alloy has been shown to enhance the mobility of minority electrons by raising the L-valley in comparison to pure GaAsSb. This decreases the number of slower electrons in the L-valley and eliminates the blocking effects at the heterojunction with InP, while still preserving the Type-II band alignment in the Γ -valley [10,11]. This improves both the high-bandwidth and high-power performance of the UTC-PDs. The simple grading-free epitaxial structure with a pure InP collector also ensures reproducible, stable, and cost-effective device manufacturing [12].

We have previously demonstrated enhanced electron transport capabilities in uniform GaInAsSb for application in high-bandwidth and high-power UTC-PDs [12–14]. In this study, we present a modified quaternary absorber comprising 100 nm of heavily doped GaInAsSb combined with 20 nm of non-intentionally doped (n.i.d) GaInAsSb absorber. The addition of the n.i.d doped GaInAsSb has improved the overall responsivity of the UTC-PDs compared to our previous design. This n.i.d absorber layer also contributed to reducing the devices' overall

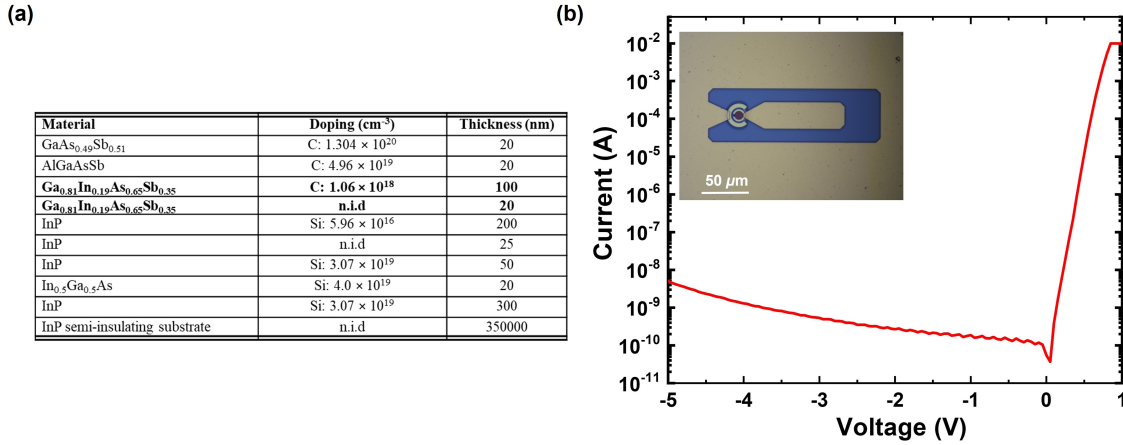


Fig. 1: (a) I - V characteristics of a $64 \mu\text{m}^2$ device size, showing low dark current. (Inset: Top-view microscopic image of a fabricated UTC-PD with the co-planar waveguide probe pads.), (b) Corresponding epitaxial layer structure of the modified UTC-PD.

capacitance and provided an additional electric field for electron transport, thereby improving the overall bandwidth of the UTC-PD. A $64 \mu\text{m}^2$ UTC-PD exhibits a zero-bias bandwidth of 60 GHz, and an output power of -11 dBm at 100 GHz, with a saturation current of 5.5 mA. At a reverse bias of 3 V, when the collector is fully depleted, the bandwidth increases to 110 GHz. This is among the best-reported photodiode bandwidth for large area device areas. The devices also exhibit a linear behavior up to 12 mA and achieved an output power of 4 dBm at 100 GHz. The devices did not show any saturation, as the saturation current was beyond our measurement capability. Regardless of that, the attained RF output power is among one of the highest reported for any standalone UTC-PDs. Given that the devices remain within the linear range, we expect to achieve higher output power for our UTC-PDs.

2. Device Fabrication and Results

The epitaxial structure of GaInAsSb/InP UTC-PDs is detailed in Fig 1 (a). The design comprises a 225 nm InP collector layer n-doped at $5.96 \times 10^{16} \text{cm}^{-3}$, a 100 nm uniform quaternary Ga_xIn_{1-x}As_ySb_{1-y} absorber doped at $1.06 \times 10^{18} \text{cm}^{-3}$, and a 20 nm non-intentionally doped (n.i.d) quaternary Ga_xIn_{1-x}As_ySb_{1-y} layer sandwiched between the absorber and collector. The composition of the absorber was selected to preserve Type-II band alignment and ensure lattice matching with the InP substrate ($x=0.81$, $y=0.65$). Photodiodes of different sizes were fabricated by optical lithography and wet etching techniques [12].

DC characterization of the photodiodes was performed using an HP4156B semiconductor parameter analyzer. The room temperature I - V characteristics of the PDs show a dark current below 10 nA up to a reverse bias of 5 V, as shown in Fig.1 (b). The measured responsivity for large area devices was 0.1 A/W at 0 V and 0.13 A/W at -3 V when the collector was fully depleted.

Two different characterization setups were used to measure the RF response in a wide range of frequencies between 0-220 GHz. The RF performance of the PDs from 0.2 to 67 GHz was characterized using a Thorlabs MX70G electrical-to-optical converter at $\lambda = 1550 \text{ nm}$ and a PNA-X vector network analyzer. A Line/Reflect/Match (LRM) coaxial calibration technique was employed using the E-Cal module N4694-60001, up to 67 GHz. The RF probe was then de-embedded to bring the reference plane to the probe tip on the output port and at the end of the RF cable at the input port. The modulator's frequency response was de-embedded from the measurement. For higher-frequency measurements up to W-Band (75 to 110 GHz) and G-Band (140 to 220 GHz), a two-tone optical heterodyne system operating at a wavelength of 1550 nm was employed to produce the RF signal. This was achieved by combining two lasers with equal amplitudes and adjusting their frequencies to create a controllable frequency offset. Both lasers were then combined using a 3-dB coupler and directed through an optical fiber onto the photodiodes. To measure the output response of the UTC-PDs, a W-band, and a G-band RF probing system was used along with VDI PM4 mm-submm power meter. The reported RF power was carefully de-embedded, accounting for a maximum insertion loss of about 1.3 dB of the WR-10 and 2 dB of WR-6 waveguide probes. The modulated light signal was amplified using an Erbium-Doped Fiber Amplifier (EDFA) and coupled onto the top-illuminated PDs using a single-mode lensed fiber.

The normalized frequency response of the given epitaxial structure is illustrated in Fig.2 (a) both at 0 V and 3 V. For a $64 \mu\text{m}^2$ device, zero-bias $f_{3\text{dB}}$ bandwidth of 60 GHz was obtained, which increased beyond 67 GHz when the collector was fully depleted at -3 V. Precise $f_{3\text{dB}}$ bandwidth of the UTC-PD, was determined upon measuring the devices up to 220 GHz. Fig.2 (b) shows the normalized RF response plotted against frequency at -3 V up to 220 GHz, showing $f_{3\text{dB}}$ bandwidth of 110 GHz. Fig.2 (c) illustrates the measured photo-generated RF output

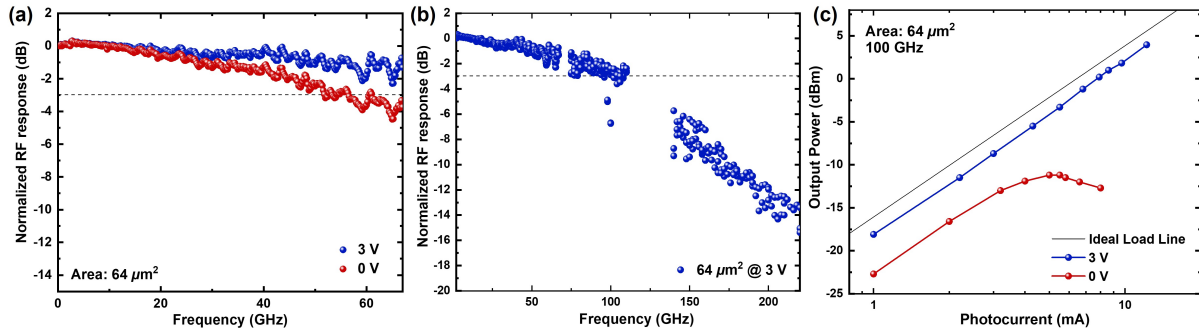


Fig. 2: (a) Measured normalized frequency response of GaInAsSb based modified UTC-PDs at -3 V and 0 V, showing $f_{3\text{dB}}$ of 60 GHz at 0 V, (b) Measured normalized frequency response of GaInAsSb based modified UTC-PDs at -3 V up to 220 GHz showing $f_{3\text{dB}}$ of 110 GHz at -3 V, and (c) The RF output power dependence of photocurrent at 100 GHz for UTC-PD at 0 V and -3 V showing saturation at 5.5 mA for 0 V and no saturation for 3 V

power plotted against the photocurrent obtained using the beating setup at 100 GHz. The graph also includes the ideal RF power under a 50 Ω load plotted against the averaged photocurrent for reference. The device shows a linear response up to a high photocurrent of 12.2 mA and an RF output power of 4 dBm. Clearly, the saturation photocurrent is well beyond 12 mA and was beyond the measurement setup capability. Despite no saturation, the reported RF power is one of the highest reported for any standalone UTC-PD. Further increases in RF power are expected with higher input optical power.

At zero-bias, the 64 μm^2 device shows a saturation photocurrent of 5.5 mA and an RF power of -11 dBm. In comparison to our regular quaternary UTC-PDs, the modified UTC-PDs show improved bandwidth, RF output power, and responsivity [12–14]. Our devices' zero-bias power performance is comparable to flip-chip bonded Type-II (GaAs_{0.5}Sb_{0.5}/InP) UTC-PDs with a modified graded collector layer of InP and In_{0.52}Al_xGa_{0.48-x}As and charge compensated GaAsSb MUTC which are designed for zero-bias performance [6, 15]. They exhibit superior power performance in comparison to Type-II MUTC, which has a saturation photocurrent of 2 mA and an RF power of -15 dBm [16], as well as Type-I GaInAs-based UTC-PD with a saturation photocurrent of 2 mA and an RF power of -18.6 dBm [3].

The present study highlights the interest in GaInAsSb absorbers in UTC-PDs due to their favorable electron transport properties using simple, easily manufacturable top-illuminated structures. The 3-dB bandwidth as well as the power performance of our quaternary UTC-PDs can be further improved by reducing the active device area and the implementation of a graded GaInAsSb absorber. Future work will also focus on improving the overall responsivity with resonant cavity structures and/or conversion to a waveguide architecture.

3. Conclusion

We have successfully demonstrated the high-bandwidth and high-power performance of Type-II GaInAsSb based modified UTC-PDs. High bandwidth of 110 GHz was observed with a linear response without RF output saturation up to a high photocurrent of 12 mA and an RF power over 4 dBm at -3V. Higher output power is expected as the devices show no saturation. The devices show a zero-bias bandwidth of 60 GHz along with a saturation photocurrent of 5.5 mA and an RF power of -11 dBm. The Type-II band alignment between GaInAsSb/InP combined with excellent electron transport allows us to achieve high power levels in the mm-wave band. Improving the overall performance of UTC-PDs by scaling down the device size and optimizing the epitaxial layers is currently underway.

References

1. T. Nagatsuma, *et al.*, Nature Photon. **10**, pp. 371 (2016).
2. H. Ito, *et al.*, IEEE J. Sel. Top. Quantum Electron., **10**, pp. 709 (2004).
3. T. Umezawa, *et al.*, in *Proc. OFC* (2015).
4. H. Ito, *et al.*, Electron. Lett., **36**, pp. 2034 (2000).
5. H. Ito, *et al.*, Electron. Lett., **36**, pp. 1809 (2000).
6. J. Wun, *et al.*, J. Light. Technol., **35**, pp. 711 (2017).
7. C. Nguyen, *et al.*, IEEE Electron Device Lett., **17**, pp. 133 (1996).
8. S. Sun *et al.*, IEEE Photon. Technol. Lett., **29**, pp. 1155 (2017).
9. L. Zheng, *et al.*, IEEE Photon. Technol. Lett., **17**, pp. 651 (2005).
10. C. R. Bolognesi and O. J. S. Ostinelli, Appl. Phys. Lett., **119**, pp. 242103 (2021).
11. W. Quan, *et al.*, IEEE Electron Device Lett., **39** pp. 1141 (2018).
12. A. M. Arabhavi *et al.*, J. Light. Technol., **39**, pp. 2171 (2021).
13. R. Chaudhary, *et al.*, in *Proc. IPC*, (2022).
14. R. Chaudhary *et al.*, in *Proc. OFC*, (2023).
15. J. S. Morgan *et al.*, J. Light. Technol., (2023).
16. F. Yu, *et al.*, J. Light. Technol., **38**, pp. 6827 (2020).